

ACOUSTICAL LETTER

Effects of airflow in constricted vocal tracts on vowel production of the reed-type artificial vocal fold

Tsukasa Yoshinaga[1,*], Takayuki Arai[2], Hiroshi Yokoyama[1] and Akiyoshi Iida[1]

[1]*Toyohashi University of Technology, 1–1 Hibarigaoka, Tempaku, Toyohashi, 441–8580 Japan*
[2]*Sophia University, 7–1 Kioi-cho, Chiyoda-ku, Tokyo, 102–8554 Japan*

(*Received 8 April 2022, Accepted for publication 17 May 2022*)

Keywords: Speech production, Aeroacoustics, Computational fluid dynamics, Artificial vocal fold, Vocal tract

1. Introduction

The human voice is produced by self-sustained oscillations of vocal folds and the resulting pulsating jet flow passing through the glottis. To mimic this sound generation mechanism, many vocal fold models have been proposed and developed for many years. The first well-known vocal fold replica, comprised of a reed and its retainer, was proposed by von Kempelen around 1780 for his speaking machine [1]. This reed-type artificial vocal fold has been still used because of its easy fabrication geometry [2]. By fabricating it with the vocal tract model of a simple tube with a cylindrical constriction, formant peaks appear in the spectrum of the generated sound like the human vowel production.

Meanwhile, the linear source-filter theory of speech production is known to become nonlinear with a constriction in the vocal tract. The shape of the vocal tract strongly affects the vocal fold vibrations. Earlier studies investigated the effects of the epilarynx [3] and bilabial fricative constrictions [4] on the vocal tracts' acoustic impedance. Additionally, computed tomography scans were performed on the oral tracts during and after tube phonation, a method for voice training and rehabilitation [5,6]. The results revealed that speakers try to keep the acoustic characteristics of the modified vocal tract geometry after the training.

Several numerical simulations have been conducted to analyze the effects of the vocal tract constrictions on the vocal fold vibration. The simulation of the three-mass body-cover model with the muscle activation control and 44-section tube vocal tract indicated that a combination of the epilarynx constriction and vocal fold adduction enhances the nonlinear effect [7]. Moreover, it was discovered that the vibration of vocal folds with a frequency near the range of the vocal tract formants induces the instability of the vibration mode [8], and this was observed in experiments [9,10]. Furthermore, the effects of the constricted vocal tract on vocal folds' contact pressures during the phonation were explored using the numerical simulation [11]. However, these numerical studies were performed with one-dimensional (1D) quasi-steady flow models, and it is still unclear whether these phenomena could be observed in the actual three-dimensional (3D) turbulent flow. The turbulent jet generated from the gap of vocal folds impinges on the constricted vocal tract walls, and this effect might change the vocal fold vibration as well as the propagating sound.

Therefore, as a preliminary study, we conduct experimental measurements and 3D flow simulations on the reed-type artificial vocal fold, which has a simpler vocal fold geometry, to clarify the effects of airflow in the constricted vocal tracts on vowel production. The reed-type vocal folds are easy to fabricate and produce similar sounds to human voices. The 3D flow simulation enables the observation of how the flow in the constricted vocal tract affects the behavior of the vocal fold vibrations. By clarifying whether this reed-type source interacts with the vocal tract in the same way as human vocal folds, we can contribute to the further development of the artificial larynx.

2. Materials and methods

2.1. Artificial vocal fold and vocal tracts

The artificial vocal fold consists of a reed and its retainer placed in a cylindrical pressure chamber (Fig. 1). By inserting airflow into the chamber, the flow passes through the flow channel between the reed and retainer, generating the sound with the reed vibration. The reed, made of polyethylene terephthalate, is 22-mm long, 10-mm wide, and 0.2-mm thick. The tip of the retainer is curved with a 30-mm radius. The cylindrical pressure chamber has a diameter of 30 mm and a length of 55 mm.

To examine the effects of the constricted vocal tract, the cylindrical vocal tract with a constriction is set at the outlet of the artificial vocal fold. The cylindrical vocal tract is called the "three-tube model" [2], and the acoustic characteristics of the vowels [i], [y], [u], [o], and [a] can be reproduced by changing the constriction position from the anterior to posterior. In this study, we used a cylinder with a total length of $L = 175$ mm, and a diameter of 34 mm which replicates the formants of general male vowels. The cylindrical constriction with a length of 50 mm was set at the anterior and posterior parts of the vocal tract. In the experiment, the diameter of the constriction d was changed every 1 mm from 7 to 13 mm. Hereafter, we call the vocal tract without the constriction "wide-wide," the constriction at the anterior part (i.e., labial constriction) "wide-narrow," and the constriction at the posterior part (i.e., epilarynx constriction) "narrow-wide," as in Ref. [7].

2.2. Experimental measurements

We conducted experiments to measure the effects of the

*e-mail: yoshinaga@me.tut.ac.jp
[doi:10.1250/ast.43.283]

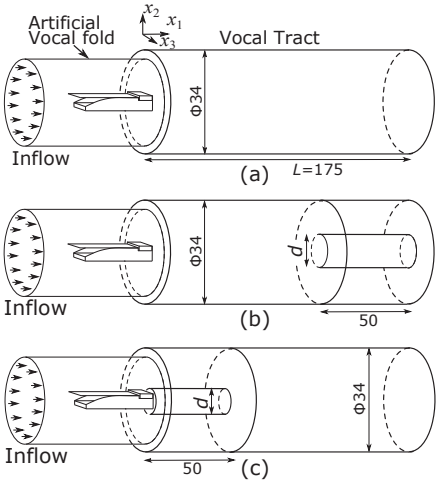

Fig. 1 Artificial vocal fold with a cylindrical vocal tract. (a) vocal tract without the constriction (wide-wide), (b) vocal tract with labial constriction (wide-narrow), and (c) vocal tract with epilarynx constriction (narrow-wide).

vocal tract constriction on the phonation threshold pressure and flow rate. The artificial vocal fold and the vocal tract were set at the center of an anechoic chamber ($V = 8.1\,\mathrm{m}^3$). A compressor (SOL-2039, Misumi, Japan) supplied steady airflow through the air tube with an inner diameter of 16 mm, and a mass-flow meter (PFM750-01, SMC, Japan). The manometer (TC-3300D, Toyo Control Co., Ltd., Japan) was set to the pressure chamber of the artificial vocal fold to measure the subglottal pressure. A flow valve (IR2000-02, SMC, Japan) was gradually opened, and the subglottal pressure and the flow rate were measured when the reed started vibrating. Additionally, to confirm the accuracy of the numerical simulation, the far-field acoustic pressure was measured using a microphone (type 4939, Brüel & Kjær, Denmark) at 100 mm from the vocal tract outlet.

2.3. Numerical flow simulation

We solved the 3D compressible Navier-Stokes equations to observe the flow and sound generation in the artificial vocal fold and tracts. To calculate the flow and acoustic fields with the moving boundaries, the volume penalization method [12] was applied to the Navier-Stokes equations. The spatial derivatives were solved using the finite difference method with a 6th-order accuracy compact scheme. The 3rd-order accuracy Runge-Kutta method was used to evaluate the time integration. This methodology enables the calculation of both fluid pressure (∼2,000 Pa) and acoustic pressure fluctuations (∼0.1 Pa).

To predict the oscillating reed geometry, the 1D beam equation was solved by coupling with the aeroacoustic field computation. The spatial derivatives of the beam equation were solved using the second-order accuracy finite difference method, and the time integration was evaluated by the second-order accuracy implicit theta-scheme [13]. As external forces, the force per unit length was obtained by integrating the pressure on the reed's surface in the spanwise-direction (axis x_3). The contact force was evaluated when the reed surface was predicted to collide with the retainer.

Structured computational grids were constructed to solve these governing equations. The minimum grid size near the reed was 0.1 mm to resolve the turbulent flow structures, and the grid size was gradually increased toward the outlet to reduce the computational costs. The maximum grid size near the acoustic sampling point (100 mm from the vocal tract outlet) was 7.9 mm, and the sound wavelength at 4,500 Hz was resolved using ten grid points. Detailed descriptions of the computational methodology can be found in Ref. [14,15].

At the inlet of the artificial vocal folds, a uniform velocity with a flow rate of $667\,\mathrm{cm}^3/\mathrm{s}$ and a pressure of 2.1 kPa was set to realize the stable reed oscillation. These values are above the phonation threshold, yet realistic as a loud voice production. At the outlet of the computational domain, the non-reflecting boundary condition was set with a buffer region that dissipates the perturbation of the pressure propagating from the vocal tract outlet. The time step of the time integration was set to 0.965×10^{-7} s, and the acoustic pressure was sampled at 100 mm from the vocal tract outlet. The acoustic pressure was sampled for 14 cycles after stable reed oscillations were attained, whereas the mean velocity and pressure along the centerline of the vocal fold and tract were calculated for the last three cycles.

3. Results

The experimentally measured phonation threshold pressure and flow rate of the artificial vocal fold with three vocal tracts are shown in Fig. 2. The onset pressure and flow rate were 696 Pa and $553\,\mathrm{cm}^3/\mathrm{s}$, respectively, for the wide-wide vocal tract. With the constriction at the lip side (wide-narrow),

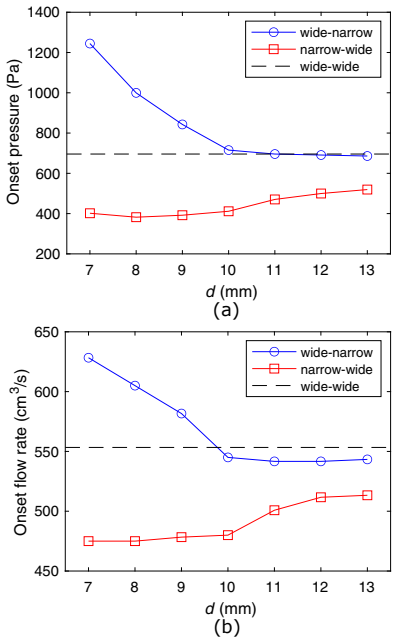

Fig. 2 Experimentally measured onset subglottal pressure at the cylindrical chamber (a), and onset flow rate passing through the reed (b) for different constriction diameters d.

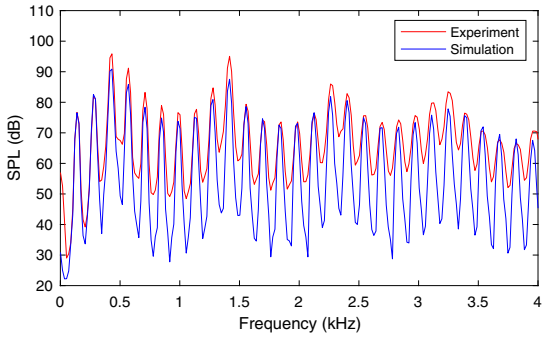

Fig. 3 Spectra of sound measured and predicted at 100 mm from the outlet of the vocal tract without constriction (wide-wide vocal tract).

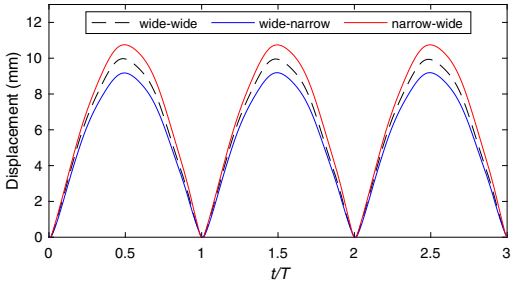

Fig. 4 Simulated reed tip waveforms with the three vocal tract conditions. The constriction diameter d was set to 8 mm for the wide-narrow and narrow-wide conditions.

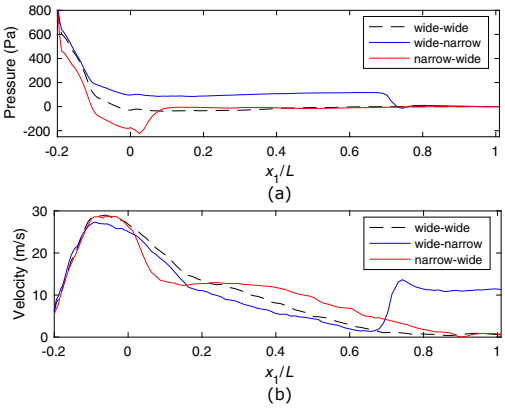

Fig. 5 Mean pressure and velocity distributions. (a) pressure and (b) velocity along the centerline of the vocal fold and tract are plotted. $x_1/L = 0$ indicates the outlet of the vocal fold, whereas $x_1/L = 1$ indicates the outlet of the vocal tract. The mean values were calculated for three reed vibration cycles.

the onset pressure was approximately 690 Pa for the constriction diameter from $d = 11$ to 13 mm, similar to that of the wide-wide vocal tract. On decreasing the constriction diameter from $d = 10$ to 7 mm, the onset pressure increased from 715 to 1,240 Pa. In contrast, with the decrease of d for the epilarynx constriction (narrow-wide), the onset pressure gradually decreased from 519 to 402 Pa. When d was decreased, the onset flow rate for the wide-narrow increased from 543 to 628 cm^3/s, whereas the onset flow rate for the narrow-wide decreased from 513 to 475 cm^3/s.

To confirm the computational accuracy of the numerical simulation, the sound spectrum measured at 100 mm in the experimental setup is compared with the predicted spectrum in Fig. 3 for the wide-wide vocal tract. The fundamental frequency fo was 139 Hz, and the amplitudes around the formant frequencies of 432, 1,417, 2,263, and 3,247 Hz were increased for both experiment and simulation. Although the peak amplitudes at the formants were underestimated by approximately 7 dB, the overall spectral shape of the simulation was consistent with that of the experiment. This result suggests that the sound generation from the flow around the oscillating reed and the acoustic resonance in the vocal tract were predicted with sufficient accuracy for the vowel evaluation.

Figure 4 shows the simulated reed tip waveforms for the vocal tracts in three cases. The constriction diameter was set to $d = 8$ mm for both wide-narrow and narrow-wide vocal tracts under the flow rate of 667 cm^3/s and the inlet pressure of 2.1 kPa. The displacement is defined as 0 when the reed is completely closed. Although the waveforms of the three vocal tract cases were almost the same, the amplitude of the wide-wide 9.95 mm decreased to 9.19 mm with the wide-narrow vocal tract, whereas it increased to 10.7 mm with the narrow-wide vocal tract.

The mean pressure and velocity in the x_1 (anterior-posterior) direction are plotted in Fig. 5 along the centerline of the vocal fold and tract. The coordinate $x_1/L = 0$ indicates the boundary between the retainer outlet and the vocal tract inlet. The mean pressure at the inlet of the vocal fold rapidly decreased toward the retainer outlet ($-0.2 < x_1/L < 0$) for all cases. With the lip constriction, the pressure in the vocal tract and retainer increased at $-0.2 < x_1/L < 0.72$, whereas the pressure in the retainer and the inlet of the vocal tract ($-0.2 < x_1/L < 0.03$) decreased with the epilarynx constriction. The pressure of -20 Pa at $x_1/L = 0$ in the wide-wide case increased to 96 Pa in the wide-narrow case and decreased to -170 Pa in the narrow-wide case.

The mean velocity increased up to 29 m/s in the retainer ($x_1/L = -0.1$) and gradually decreased toward the vocal tract outlet of the wide-wide case. On adding the constriction at the lip, the mean velocity increased up to 13 m/s in the constriction ($0.72 < x_1/L < 1$), and the velocities upstream from the constriction ($-0.09 < x_1/L < 0.72$) became smaller than those in the wide-wide vocal tract because the jet spread in the wider region. In contrast, with the constriction at the epilarynx, the velocities increased from the middle of the constriction to the outlet of the vocal tract ($0.2 < x_1/L < 0.9$).

4. Discussion and conclusions

The experimental measurements showed that the vocal tract constriction significantly affects the phonation threshold pressure and flow rate of the reed-type artificial vocal fold. With the lip constriction from $d = 7$ to 9 mm, the onset pressure and flow rate increased from those of the wide-wide

vocal tract, whereas the onset pressure and flow rate decreased on constricting the epilarynx from $d = 7$ to 13 mm. These results suggest that the artificial vocal fold oscillates with smaller inflow energy for the epilarynx constriction (i.e., more efficient). This effect is consistent with the results of previous numerical studies [7,11]. In contrast, phonations with lip constriction require more flow energy for the reed oscillation to start.

The proposed numerical simulations demonstrated that the lip constriction decreased the reed vibration amplitudes, whereas the epilarynx constriction increased the reed amplitudes. This result agrees with the fact that voice training and therapy with the semi-occluded vocal tract of the lip constriction reduces the vocal folds' collision stress [7]. The vocal tract constriction significantly affected the mean pressure in the retainer ($x_1/L = 0$), and the lip constriction decreased the pressure difference between the chamber inlet and the retainer outlet. Hence, the lip constriction reduced the reed oscillation's driving force. In contrast, the epilarynx constriction increased the velocity at the retainer outlet, resulting in a pressure drop in the retainer and amplification of the reed's driving force. These results also explain the changes in the phonation thresholds with different constriction diameters. The increase of the supraglottal pressure due to the smaller lip constriction increases the onset pressure, whereas the decrease of the supraglottal pressure with smaller epilarynx constrictions reduces the onset pressure.

In conclusion, we examined the effects of the vocal tract constriction on vowel production with the simplified geometry and found that nonlinear effects similar to the human vocal folds can be observed with the reed-type artificial vocal fold. Additionally, although the simulation considered 3D flow turbulence, the increase and decrease of the supraglottal pressures, which changed the oscillation driving force, were observed to be similar to the conventional 1D acoustic modeling of the vocal folds [7–11]. However, it should be noted that the difference in the vibratory patterns between the reed-type vocal fold and the actual human vocal fold may cause some discrepancies in the results. Future work is expected to apply the same aeroacoustic simulation methodology to more realistic vocal fold and tract geometries to observe peculiar conditions involving the 3D flow interactions.

Acknowledgements

This work was supported by JSPS KAKENHI, Grant number: JP18K02988; JP20K14648; JP21K02889. We acknowledge Dr. Ken-ichi Sakakibara for his insightful comments and discussion on this study.

References

[1] H. Dudley and T. H. Tarnoczy, "The speaking machine of Wolfgang von Kempelen," *J. Acoust. Soc. Am.*, **22**, 151–166 (1950).
[2] T. Arai, "Sliding three-tube model as a simple educational tool for vowel production," *Acoust. Sci. & Tech.*, **27**, 384–388 (2006).
[3] I. R. Titze and B. H. Story, "Acoustic interactions of the voice source with the lower vocal tract," *J. Acoust. Soc. Am.*, **101**, 2234–2243 (1997).
[4] B. H. Story, A. M. Laukkanen and I. R. Titze, "Acoustic impedance of an artificially lengthened and constricted vocal tract," *J. Voice*, **14**, 455–469 (2000).
[5] T. Vampola, A. M. Laukkanen, J. Horáček and J. G. Švec, "Vocal tract changes caused by phonation into a tube: A case study using computer tomography and finite-element modeling," *J. Acoust. Soc. Am.*, **129**, 310–315 (2011).
[6] M. Guzman, A. M. Laukkanen, P. Krupa, J. Horáček, J. G. Švec and A. Geneid, "Vocal tract and glottal function during and after vocal exercising with resonance tube and straw," *J. Voice*, **27**, 523.e19–523.e34 (2013).
[7] I. R. Titze, "Voice training and therapy with a semi-occluded vocal tract: Rationale and scientific underpinnings," *J. Speech Lang. Hear. Res.*, **49**, 448–459 (2006).
[8] I. R. Titze, "Nonlinear source–filter coupling in phonation: Theory," *J. Acoust. Soc. Am.*, **123**, 1902–1915 (2008).
[9] T. Kaburagi, M. Ando and Y. Uezu, "Source-filter interaction in phonation: A study using vocal-tract data of a soprano singer," *Acoust. Sci. & Tech.*, **40**, 313–324 (2019).
[10] K. Migimatsu and I. T. Tokuda, "Experimental study on nonlinear source–filter interaction using synthetic vocal fold models," *J. Acoust. Soc. Am.*, **146**, 983–997 (2019).
[11] Z. Zhang, "Vocal tract adjustments to minimize vocal fold contact pressure during phonation," *J. Acoust. Soc. Am.*, **150**, 1609–1619 (2021).
[12] Q. Liu and O. V. Vasilyev, "A Brinkman penalization method for compressible flows in complex geometries," *J. Comput. Phys.*, **27**, 946–966 (2007).
[13] F. Avanzini and M. Van Walstijn, "Modelling the mechanical response of the reed-mouthpiece-lip system of a clarinet. Part I. A one-dimensional distributed model," *Acta Acust. united Ac.*, **90**, 537–547 (2004).
[14] T. Yoshinaga, T. Arai, R. Inaam, H. Yokoyama and A. Iida, "A fully coupled fluid–structure–acoustic interaction simulation on reed-type artificial vocal fold," *Appl. Acoust.*, **184**, 108339 (2021).
[15] T. Yoshinaga, H. Yokoyama, T. Shoji, A. Miki and A. Iida, "Global numerical simulation of fluid-structure-acoustic interaction in a single-reed instrument," *J. Acoust. Soc. Am.*, **149**, 1623–1632 (2021).